3

Temperature-Dependent Optical Properties of Colloidal IV-VI Quantum Dots, Composed of Core/Shell Heterostructures with Alloy Components

Efrat Lifshitz, Georgy I. Maikov, Roman Vaxenburg, Diana Yanover, Anna Brusilovski, Jenya Tilchin and Aldona Sashchiuk
Schulich Faculty of Chemistry, Russell Berrie Nanotechnology Institute, Solid State Institute, Technion, Haifa, Israel

1. Introduction

Colloidal semiconductor nanocrystals attract worldwide scientific and technological interest due the ability to engineer their optical properties by the variation of size, shape, and surface properties.[1-3] Recent studies revealed new strategies related to composition control of the properties, including alloying,[4-7] doping,[8] and in particular the formation of core/shell heterostructures.[9-14] Whereas major effort has been devoted to the development of II-VI core/shell structures,[12-15] there are only a few reports concerning the heterostructures of IV-VI (PbSe, PbS) colloidal quantum dots (CQDs).[16-19] PbSe, PbS and $PbSe_xS_{1-x}$ alloyed CQDs are the focus of widespread interest due to their unique electronic and optical properties, with feasibility of applications in near infra-red (NIR) lasers, photovoltaic solar cells, Q-switches and nano-electronic devices.[20] These semiconductors have a simple cubic crystal structure with nearly identical lattice constants 5.93 Å and 6.12 Å at 300 K, respectively, which facilitates the formation of hetero-structures. Recently, high quality PbSe/PbS core/shell[16-19] and completely original $PbSe/PbSe_xS_{1-x}$ core/alloyed shell CQDs structures[19] were produced using a single injection process, offering the potential to tailor the crystallographic and dielectric mismatch between the core and the shell, forming a perfect crystalline hetero-structure. These structures present higher photoluminescence (PL) quantum yield (QY) with respect to those of core CQDs and tunability of the band-edge offset with variation of the shell thickness and composition, eventually controlling the electronic properties of the CQDs.

During the past few years, considerable interests have been focused on the thermally activated processes of the ground-state exciton emission of PbSe core CQDs.[21] The variation of the PL properties with temperature showed two thermal activation thresholds: the first in the temperature range 1.4–7 K connected with activation of acoustic phonon assisted dark exciton decay, and the second in the temperature range 100–200 K, connected with activation of bright excitons. This study also shows that the temperature coefficient of the

energy gap and the optical phonon coupling were reduced with the decrease of the diameter, while the acoustic phonon coupling grew with the decrease of the diameter. Since the first report of experimentally prepared PbSe/PbS core-shell CQDs, some simple physical properties, such as electronic structure had been studied.[22] The previous theoretical work predicted a variation of the electronic structure of PbSe/PbS CQDs, pronounced in the variation of the carriers' radial distribution function, with the variation of the core-radius/shell-thickness ratio, showing a significant separation of the electron and hole wave functions only when the shell-thickness becomes equivalent or larger than the core radius. However, the electronic structure and optical properties of colloidal IV-VI quantum dots, composed of core/shell heterostructures with alloy components still lack systematic and in depth study.

Considering the significant potential of the IV-VI heterostructures the present work describes the structural and temperature-dependent optical characterization of PbSe/PbS core/shell (c/sh), PbSe/$PbSe_xS_{1-x}$ core/alloyed-shell (c/a-sh), and newly prepared $PbSe_yS_{1-y}$/ $PbSe_xS_{1-x}$ alloyed-core/alloyed shell (a-c/a-sh) CQDs,[23] with variable internal diameters and a radial gradient composition (when $0 < x < 1$, $0 < y < 1$) with respect to those of pure PbSe and PbS CQDs. The investigated CQDs were prepared by colloidal chemistry. The structure and composition of the CQDs were characterized by the use of high-resolution transmission electron microscopy (HR-TEM), selected area electron diffraction (SAED), energy-dispersive analysis of X-ray (EDAX). A thorough investigation of the optical properties was performed by following the variable temperature continuous-wave (cw) and transient (temporal and spectrally resolved) PL spectra, exploring energy shift, band edge temperature coefficient, alleviation of a dark-bright splitting (or exchange interaction), valley-valley interaction, emission QY, and radiative lifetime of the heterostructures, in comparison with the existing properties of the primary PbSe core CQDs[21] and PbS CQDs with equevalent size.[24]

This chapter is organized as follows. Section 2 presens the significant effect of thermally activated processes of the ground-state exciton emission of various $PbSe_xS_{1-x}/PbSe_yS_{1-y}$ a-c/a-sh CQDs structures, suggesting that cw-, temporal and spectrally resolved PL of PbSe/PbS (c/sh) , PbSe/$PbSe_xS_{1-x}$ (c/a-sh) and $PbSe_yS_{1-y}/PbSe_xS_{1-x}$ a-c/a-sh CQDs over a wide range of temperatures have distinguished properties in comparison with those of pure PbSe core CQDs with equivalent overall size (R_s) and identical core radius (R_c). Section 3 discusses the thermally activated processes of PL in PbS CQDs, while the theoretical insight into the electronic band structure of graded $PbSe_yS_{1-y}/PbSe_xS_{1-x}$ a-c/a-sh QDs structure with different composition and/or size using the multiband $\mathbf{k}\cdot\mathbf{p}$ envelope function method is given in Section 4. Section 5 presents the colloidal synthesis procedures and **e**xperimental techniques, used for CQDs structural and spectroscopic characterizations**.**

2. Temperature influence on composition-tunable optical properties of $PbSe_yS_{y-1}/PbSe_xS_{1-x}$ c/sh CQDs.

The investigated CQDs were prepared by colloidal chemistry, according to the short description given below in Section 5.1 and a detailed procedure reported in.[19] Figure 1 represents HR-TEM images of $PbSe_{0.5}S_{0.5}/PbSe_{0.27}S_{0.73}$ (a) and PbSe/PbS (b) CQDs.

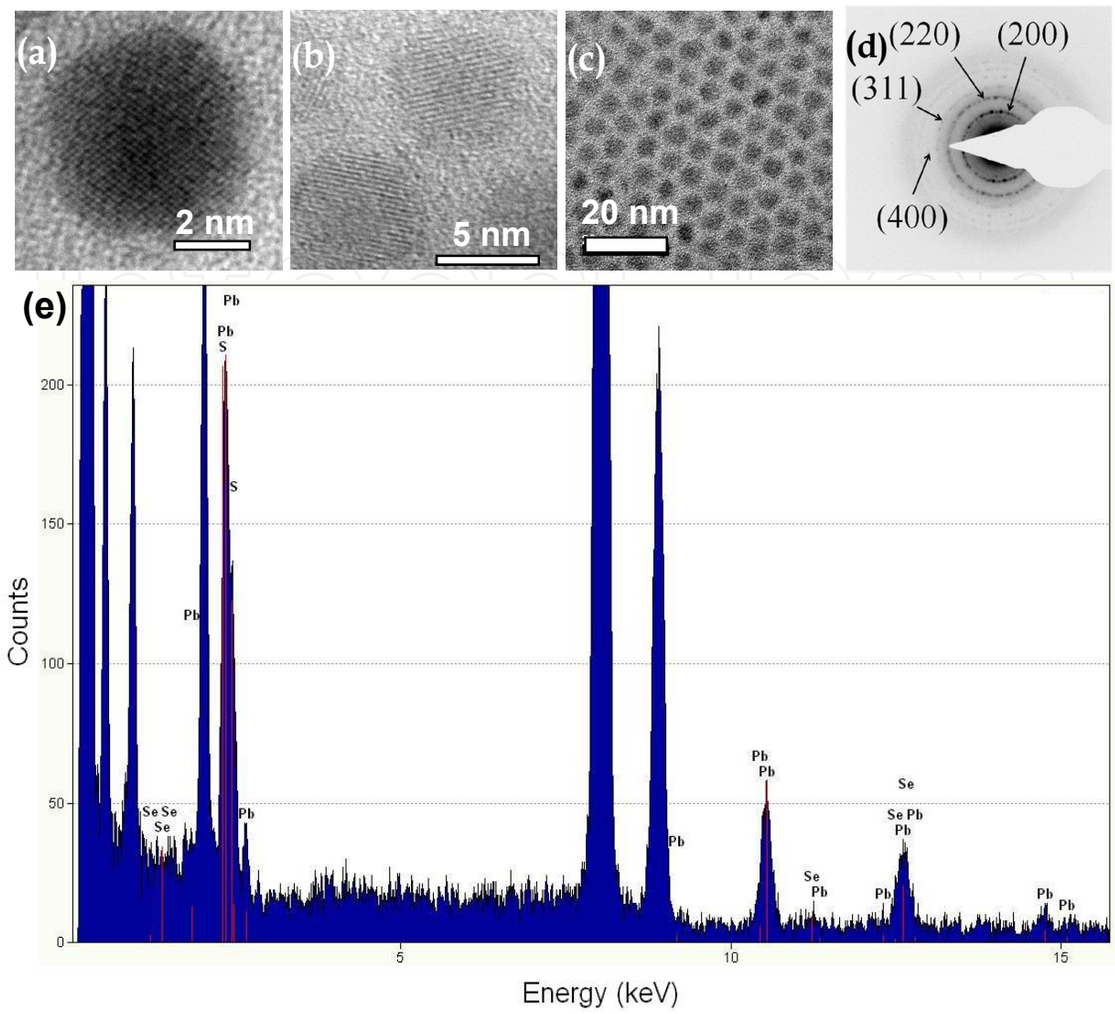

Fig. 1. Representative HR-TEM image of: single $PbSe_{0.5}S_{0.5}/PbSe_{0.27}S_{0.73}$ a-c/a-sh CQD with R_s of 2.0 nm (a), PbSe/PbS c/sh CQD with R_c of 1.3 nm and R_s of 2.5 nm (b), TEM image of an ensemble of CQDs shown in (a) (c), SAED image of the CQDs in (c) (d), EDAX spectrum of $PbSe_{0.5}S_{0.5}/PbSe_{0.27}S_{0.73}$ a-c/a-sh CQDs (e).

These images reveal distinguished crystal planes, supporting high crystallinity of the a-c/a-sh CQDs. In most cases the core/shell interface is indistinguishable in $PbSe_{0.5}S_{0.5}/PbSe_{0.27}S_{0.73}$ CQD (Panel (a)) due to the close proximity of the crystallographic components of PbSe and PbS semiconductors. However, a boundary is noted in PbSe/PbS CQD with a shell width > 3 nm (Panel (b)). A representative TEM image of CQDs shown in (a) is presented in Panel (c), exhibiting a size uniformity of ~ 5%. A representative SAED of CQDs shown in (c) is shown in Panel (d), confirming a rock-salt crystallographic structure ($Fm\bar{3}m$ space group). Similar rock-salt structures appeared in all the investigated samples. Representative EDAX spectra are presented in Panel (e). The Pb, Se, and S percentages of various samples are listed in Table 1.

Representative absorption (dashed lines) and cw-PL (solid lines) spectra of a few samples with various composition and size, measured at room temperature (RT) are shown in Figure 2.

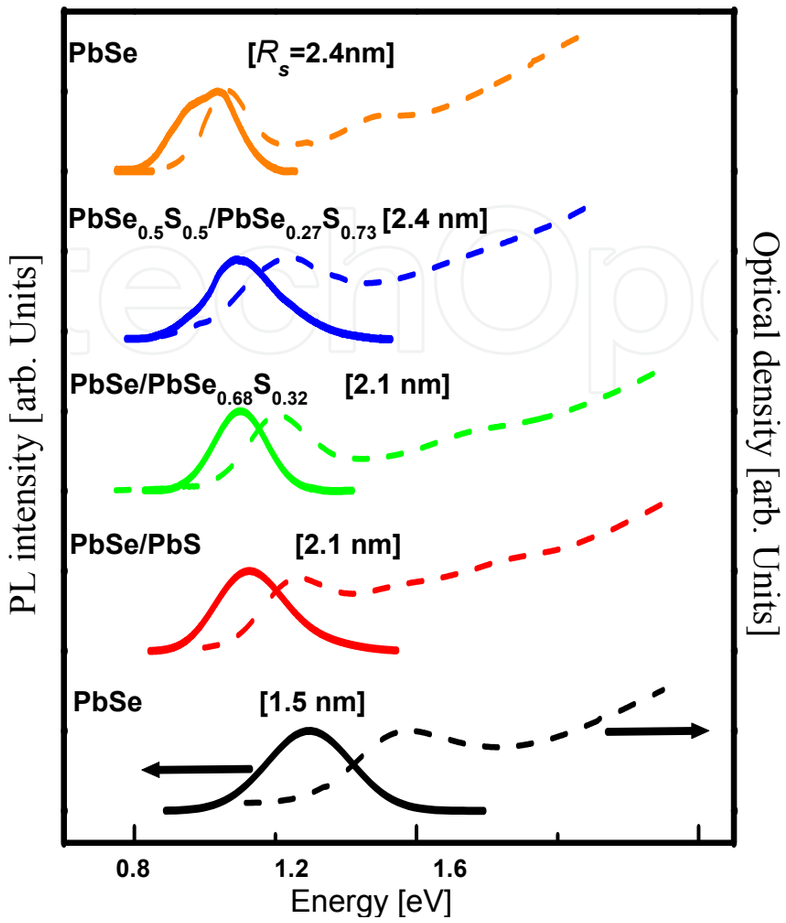

Fig. 2. Absorption (dashed lines) and emission (solid lines) spectra of PbSe core (bottom and top curves), PbSe/PbS c/sh, PbSe/$PbSe_{0.68}S_{0.32}$ c/a-sh and $PbSe_{0.5}S_{0.5}/PbSe_{0.27}S_{0.73}$ a-c/a-sh CQDs with overall radius, R_s, as labeled in the figure and measured at RT. The core radii of the heterostructures presented are in accordance with Table 1.

The bottom and top curves correspond to the spectra of PbSe core CQDs with average radius of R_S = 1.5 nm and 2.4 nm, respectively. The middle curves represent different heterostructures (c/sh, c/a-sh and a-c/a-sh), with composition and size as labeled in the Panel, when R_c = 1.5 nm and R_s up to 2.4 nm. These sets of curves suggest the occurrence of a red-shift of the absorption and emission spectra of the heterostructures with respect to those of the primary cores with R_S = 1.5 nm, but they are blue shifted with respect to that of pure PbSe cores with R_S = 2.4 nm. This midway shift is related to a quantum size effect combined with a composition tuning of the band edge energy.

The experimental band gap energy (E_g), estimated by the first excitonic absorption band, and the corresponding calculated values (discussed below) of the studied materials are listed in Table 1. The table also designates the PL quantum yield (η) of a few selected samples. The determination of the η is given in detail in the Section 5.3. Systematic improvement (up to 88%) of the η was found in c/sh, c/a-sh and a-c/a-sh CQDs *versus* those of the primary core CQDs. The relatively high η might be related to the improved

quality of surfaces, *e.g.*, close crystallographic match between PbSe core and PbS or $PbSe_xS_{1-x}$ shell, as well as the increase of the sulfur precentege at the exterior surface, with a lower oxidation outcome. The cw-PL spectra shown in Figure 2 were pumped by a nonresonant excitation (1.54 eV), showing an asymmetric or a split band, Stokes shifted with respect to the first absorption band by an energy, E_s, as listed in Table 1.

Molecular formula of CQDs	Pb [%]	Se [%]	S [%]	R_c [nm]	R_s [nm]	E_g exp. [eV]	E_g calc. [eV]	η [%]	τ_{rad} [μs]	E_s [meV]
PbSe	51.5	48.5	0.0	1.5	1.5	1.17	1.03	48	2.99	112
PbSe	54.0	46.0	0.0	2.4	2.4	0.93	1.16	83	1.23	34
PbSe/PbS	55.2	17.1	27.7	1.5	2.1	1.03	1.10	65	2.62	55
PbSe/PbS	53.8	13.5	32.7	1.5	2.3	0.98	0.95	88	1.72	53
$PbSe/PbSe_{0.68}S_{0.32}$	50.0	40.0	10.0	1.5	2.1	1.00	1.14	68	2.21	75
$PbSe_{0.5}S_{0.5}$	50.8	25.1	24.2	1.6	1.6	1.18	1.30	27	5.50	103
$PbSe_{0.5}S_{0.5}/PbSe_{0.24}S_{0.76}$	49.2	20.3	30.5	1.6	1.9	1.09	1.10	46	2.37	73
$PbSe_{0.5}S_{0.5}/PbSe_{0.27}S_{0.73}$	48.8	17.5	33.7	1.6	2.4	1.02	0.97	65	1.96	45

Table 1. Relevant parameters of the investigated CQDs; Pb, Se, S percentages, core radius (R_c), overal radius (R_s), band gap energy (Eg), quantum yield (η), radiative lifetime (τrad) and Stokes shift (Es), all at RT.

Figure 3 compares the PL emission Stokes shift energy versus the experimental band gap energy, corresponding to the first excitonic absorption band of PbSe (black squares), PbSe/PbS c/sh (red circles) with primary R_c of 1.5 nm, $PbSe/PbSe_{0.8}S_{0.2}$ c/a-sh (green triangles) with primary R_c of 1.5 nm and $PbSe_{0.6}S_{0.4}/PbSe_{0.17}S_{0.83}$ a-c/a-sh (blue diamond's) with $PbSe_{0.6}S_{0.4}$ core radius of 1.5 nm CQDs at RT. The nonresonant Stokes shift has an interesting behavior: (i) a reduction of E_s in c/sh heterostructures with respect to their primary cores. The Stokes shift is related to a total growth of R_s with respect to R_c , as well as to the generation of an exciton fine-structure by valley-valley and electron-hole exchange interactions. These interactions may be reduced in c/sh structures, due to a *quasi*-type-II band alignment, as will be discussed below; (ii) E_s in c/a-sh and a-c/a-sh CQDs is smaller than in the corresponding cores, however, larger than that in core or c/sh CQDs of an equivalent size (see Table 1). Similar increase of E_s, in alloyed CQDs (in comparison with pure cores) was observed before in II-VI[5, 25] and III-V[26] quantum dots, and was associated with a nonlinear effect such as optical bowing, induced by a lattice constant deformation or different carriers' distribution in alloyed materials.[5]

Figure 4 illustrates the evolution of the cw-PL spectra of a few samples, excited at 1.54 eV and recorded at different temperatures from 1.4 K to 300 K as shown by the ruler in the figure. Panels (a) and (e) represent the spectra of reference PbSe cores, with an average radius, R_S = 1.5 nm and 2.4 nm, respectively. The CQDs were desperse in glass solution (GS). The cw-PL spectra correspond to a band edge exciton recombination emission at the L-point of the Brillouin zone of a PbSe semiconductor. Panels (b) and (c) show the spectra of

PbSe/PbS c/sh and PbSe/$PbSe_{0.68}S_{0.32}$ c/a-sh CQDs, respectively, both with R_c = 1.5 nm and R_s = 2.1 nm. Panel (d) exhibits the spectra of $PbSe_{0.5}S_{0.5}$/$PbSe_{0.27}S_{0.73}$ a-c/a-sh CQDs with R_s = 2.4 nm. Once again, at all temperatures, the emission energy of the heterostructures shows a midway shift between the emission energy of small and large reference cores (Panels (a) and (e)). The cw-PL spectra of the smallest PbSe cores CQDs are dominated by a single exciton band over the entire temperature range, similar to the observation found in Ref.[21]. However, the emission spectra of the larger PbSe cores occasionally exhibit a split band at elevated temperatures.

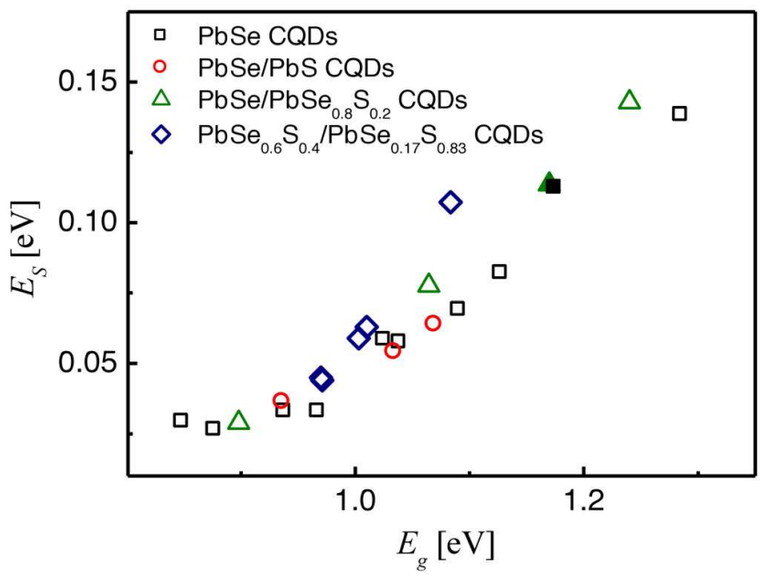

Fig. 3. Plot of the emission energy Stokes shift E_s versus E_g of the CQDs designated at the legend of the Figure, at RT. The full black square correspond to the primary core of the PbSe/PbS CQDs and the full green triangle corresponds to the primary core of the PbSe/$PbSe_8S_{0.2}$ CQDs.

Identicaly the cw-PL spectra of the various heterostructures show an asymmetric or a split shape at all temperatures, presumably consisting of two overlapping emission bands, where the energy split is of the order 30-55 meV, decreasing with the increase of the shell width and the S/Se ratio (see Figure 4). For convenience, we fitted the spectra to a sum of two Gaussian emission bands as demonstrated in Figure 5 for a $PbSe_{0.5}S_{0.5}$/$PbSe_{0.27}S_{0.73}$ a-c/a-sh sample at three representative temperatures (5 K, 150 K and 300 K). Interestingly, the split energy closely retains its value upon the increase in temperature, although the high energy component is gaining intensity with the increase in temperature. As a simple test of the possibility that the split band arises due to traps or defects on the surface of the CQDs, we checked the pumping intensity dependence of the spectra, as traps and defects should be saturated at high enough energies. We found that the spectrum not only maintained its shape but also the relative intensity between the two bands remained constant, while the pumping intensity varied over 10 orders of magnitude. The possibility of experimental artifacts was also rejected as the dual band still appears after intensity calibration on the experimental system and at different energies for different samples (core, c/sh, c/a-sh and

a-c/a-sh). We take this evidence as proof that the dual band is an intrinsic property of the electronic structure of the samples.

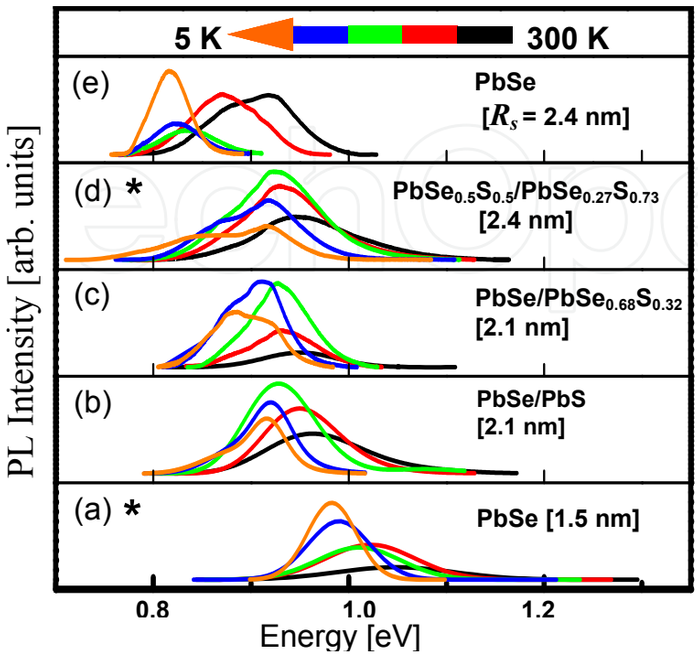

Fig. 4. cw-PL spectra of: PbSe core CQDs with core radius of R_S = 1.5 nm (a) and R_S = 2.4 nm (e); PbSe/PbS c/sh (b) and PbSe/$PbSe_{0.68}S_{0.32}$ c/a-sh CQDs (c), both with R_c = 1.5 nm and R_s = 2.1 nm; $PbSe_{0.5}S_{0.5}$/$PbSe_{0.27}S_{0.73}$ a-c/a-sh CQDs (d) with R_c = 1.6 nm and R_S = 2.4 nm. The CQDs were dispersed in GS. The data were recorded at various temperatures shown by the ruler. (* the PL intensity was multiplied by a factor of 3 at RT).

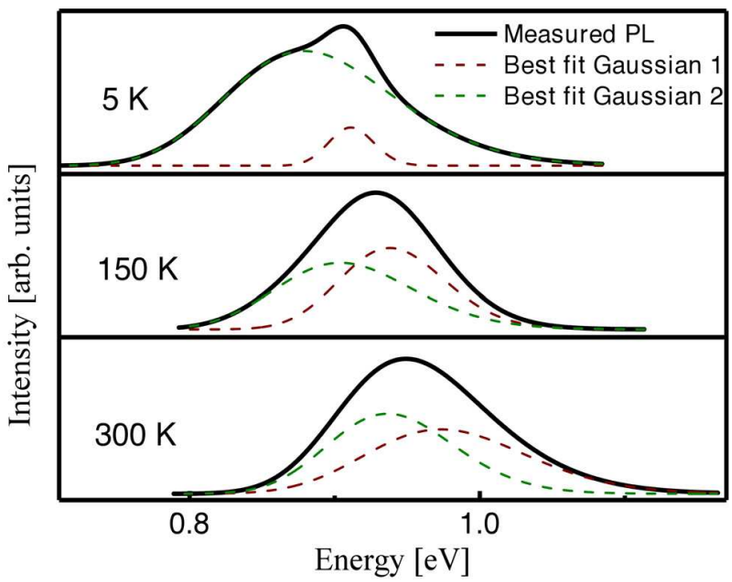

Fig. 5. PL spectra (black) and its best fit Gaussian curves (green and red) for $PbSe_{0.5}S_{0.5}$/$PbSe_{0.27}S_{0.73}$ a-c/a-sh CQDs, recorded at 5 K, 150 K and 300 K.

The splitting might be related to the occurrence of a recombination emission from two low lying excited states based on the following grounds: (i) a break of the four-fold degeneracy at the Brillouin L-point minima in IV-VI rock-salt structures, by confinement or valley-valley interaction. Indeed, valley-valley interaction, previously reported,[27-29] suggested a split of the band edge into two manifolds, each composed of bright and dark states induced by exchange interaction. The valley-valley split energy is in the range of 20-60 meV, increasing with the decrease of the CQDs' size, close to the experimental values attained in this work, which also increased with the reduction of R_s; (ii) simultaneous emission from both a dark and bright states, if a Boltzmann distribution at the cryogenic temperatures permits a heavy population of the higher energy bright state. This case is less probable, since the observed split of a few tenths of meV is substantially larger than a theoretical reported value for an exchange splitting between dark and bright states in pure PbSe cores; (iii) two emission processes can be related to parallel radiative recombination of a type-I and *quasi*-type II transitions, overlapping in an ensemble of CQDs. Presumably, such a case can be excluded, based on the observed uniformity, size and composition; (iv) occurrence of energy transfer between subgroups of small and large CQDs. The examined CQDs were dissolved in glass solutions, with a relatively low concentration, minimizing the energy transfer process. Thus, valley-valley interaction is the most probable mechanism for a split emission band.

The ΔE between the two bands for different samples are listed in Table 2. The table designates a general trend, a decrease of the ΔE with the increase of the R_s of the CQDs as well as the similarity in the value of ΔE of core CQDs and c/sh (or c/a-sh) CQDs of similar R_s (although their first exciton emission occurs at different energies).

Molecular formula	R_c [nm]	R_s [nm]	ΔE [meV]
PbSe	1.5	1.5	-
PbSe	2.0	2.0	53.1
PbSe	2.2	2.2	53
PbSe	2.4	2.4	52.6
PbSe/PbS	1.5	1.8	70.1
PbSe/PbS	1.5	2.1	59.1
PbSe/PbS	1.5	2.4	54.9
PbSe	1.5	1.5	67.3
$PbSe/PbSe_{0.68}S_{0.32}$	1.5	2.1	55.3
$PbSe/PbSe_{0.75}S_{0.25}$	1.5	2.5	49.2
$PbSe_{0.5}S_{0.5}$	1.6	1.6	63.4
$PbSe_{0.5}S_{0.5}/PbSe_{0.24}S_{0.76}$	1.6	1.9	43.2
$PbSe_{0.5}S_{0.5}/PbSe_{0.27}S_{0.73}$	1.6	2.4	40.1

Table 2. Splitting energy ΔE of the PL emission spectra in PbSe core, PbSe/PbS c/sh, $PbSe/PbSe_xS_{1-x}$ c/a-sh and $PbSe_yS_{1-y}/PbSe_xS_{1-x}$ a-c/a-sh CQDs at RT.

The nature of the two emitting states in PbSe CQDs have recently been investigated theoretically[27, 30] and exsperimentally[21, 23, 29, 31-33]. These studies have suggested that splitting within the exciton fine structure near the band gap may be responsible[23, 27, 29]. We proposed that the problem of two emitting bands need supplementary evidence, which can be gained from the temporal and spectrally resolved PL measurements.

The transient PL spectra were measured by exciting the sample with 1.17 eV and following the decay time (τ_0) of the emission intensity. Figure 6(a) displays decay curves of the samples given in the legend, measured at RT, monitoring the low energy PL component. Predominantly, the curves exhibit a single exponent behavior, where the value of τ_0 decreases upon the growth of a core radius from R_s = 1.5 nm to 2.4 nm. However, the τ_0 of the c/sh CQDs is longer than that of the primary PbSe cores. Spectrally resolved transient PL measurements provide more evidence of the two PL band nature. Plots of the values of τ_0 measured at various temperatures (as indicated by the arrow), monitored across the PL spectrum of PbSe cores and PbSe/PbS c/sh CQDs, are shown in the inset of Figure 6(a). The symbols are the experimental points and the solid lines are to guide the eye. It shows that the τ_0 of the core CQDs is approximately invariant across the PL spectrum. However, there is a pronounced decrease of the τ_0 when moving from the red to the blue side of a PL spectra of a c/sh sample, mainly pronounced at low T, but becoming insensitive to the detection energy at RT. The variation of τ_0 across the PL band supports the existence of emission of at least two manifold of states in the PL spectrum of the heterostructures, involving different radiative transitions, each of which having a distinct dependence on the temperature. τ_0 is correlated to the PL radiative lifetime (τ_{rad}) by the Eq. $\tau_{rad} = \tau_0/\eta$ (η values are given in Table 1). Considering this relations, Figure 6(b) represents plots of τ_{rad} *versus* the measured T of the samples given in the legend of Panel (a), monitored only on the low energy PL component.

These plots reveal a drastic decrease of τ_{rad} with the increase in T in core and c/sh CQDs, related to a dark exciton emission,[21] however, only a minor change in c/a-sh and a-c/a-sh CQDs. The small variation of τ_{rad} in the later CQDs is also related to the diminished climax in the PL intensity versus *1/T* (see Figure 7(b)). Both effects suggests elevation of the dark exciton characteristic in alloyed CQDs. Figure 6(c) compares plots of τ_{rad} versus R_s of core and c/sh CQDs at three different T (5 K, 100 K and 300 K). These curves reflect a common behavior, characterized by a reduction which is turned into an extension of τ_{rad} with the increase in R_s (called bowing effect). The turning points are mainly pronounced when measured at low T. It is important to note that the decay processes in c/a-sh samples resemble those of the c/sh materials (not shown), but the turning points in c/sh and c/a-sh CQDs occur at a smaller R_s than that of cores of equivalent size. In fact, a turning point in the variation of τ_{rad} with size was already reported in PbSe core CQDs at RT for samples with R_S between 2 nm to 10 nm. Currently the mechanism of this behavior is not clearly understood, however it was previously suggested[24, 34] that the initial reduction of τ_{rad} with increasing size could be attributed to the size-dependence of the matrix element for spontaneous emission $\left|\left\langle \psi_f \left| \hat{\mathbf{p}} \right| \psi_i \right\rangle\right|^2$ which governs the recombination rate up to $R_s \approx 2$ nm.[35] For larger sizes, however, the matrix element is expected to become size-independent, so τ_{rad} becomes proportional to the wavelength of emitted radiation, which is consistent with the trend observed in Figure 6(c).

Figure 7(a) displays the temperature variation of the peak emission of the low energy cw-PL band of a few heterostructures, large core and small reference core, as given in the legend. The Figure demonstrates the peak energy at T, relative to that at 1.4 K (E_{PL}(T)-E_{PL}(1.4 K)), *versus* T. The plots disclose a blue-shift of the emission energy with increase in T, which is largest for PbSe cores; however, they illustrate a moderate change in the heterostructures. The symbols designate the experimental points, and the solid lines are best fitted curves. A tangent line to the fitted curve evaluates the slope, revealing the temperature coefficient,

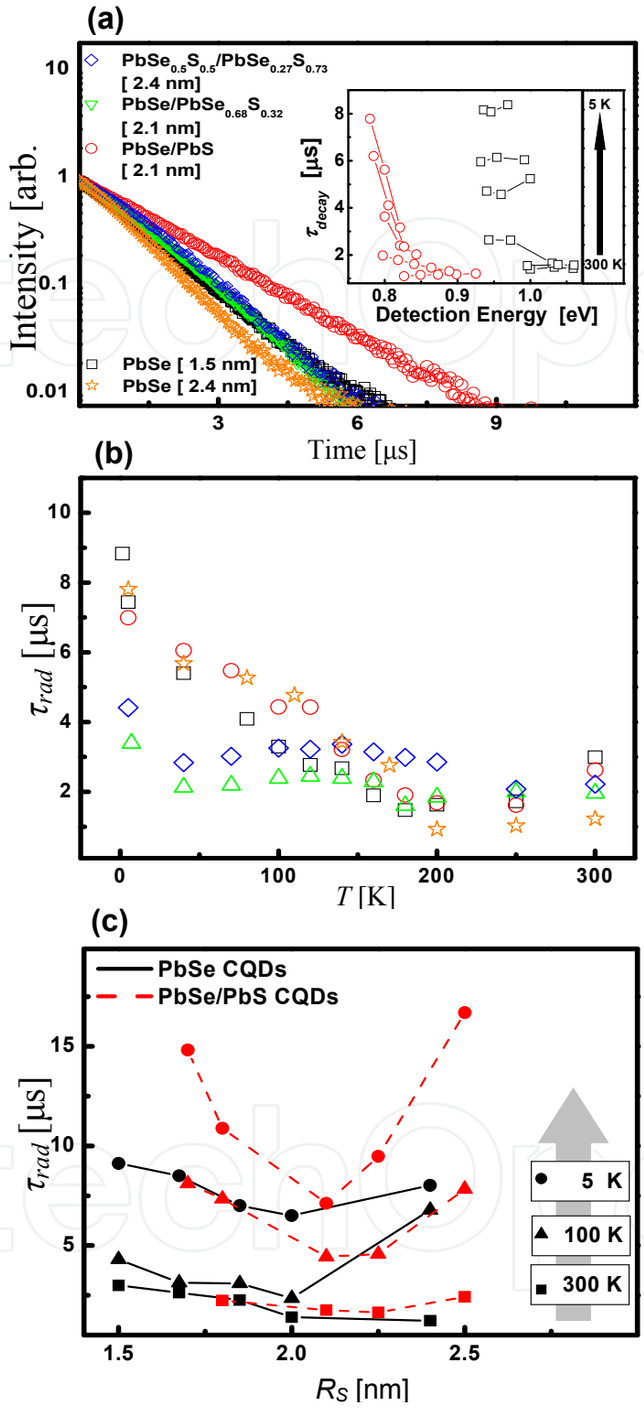

Fig. 6. Representative PL decay curves of the samples listed in the legend at RT (a); The inset in (a) presents plots of the measured τ_0 versus the detection energy across the PL spectrum, of core and c/sh CQDs, measured at different temperatures (5-300 K) as indicated by the arrow; Variation of the radiative lifetime versus the temperature of the samples listed in Panel (a) (b); Plots of the radiative lifetime versus the radius (R_s) of cores (solid line) and the corresponding c/sh (dashed line) CQDs, measured at the various temperatures as indicated in the figure (c).

dE/dT. This coefficient is most commonly derived from the temperature dependence of the first excitonic transition energy, using Varshni[36] relation, however, if the emission Stokes shift is invariant under the temperature, the coefficient derived in the present case should be relatively close to the band edge value, dE_g/dT. The best fitted coefficients of a few samples are listed in Table 3, indicating an increase of *dE/dT* with an increase in size[37] approaching the bulk value of dE_g/dT. Also, those coefficients of the heterostructures are reduced with respect to pure cores of equivalent R_s, which are mostly pronounced in a-c/a-sh CQDs. The temperature dependence of the coefficient dE_g/dT has dominant contributions from crystal dilation and electron-phonon interactions, as well as minor contributions from mechanical strain and thermal expansion of the wavefunction envelope.[37] Since the thermal expansion coefficients of bulk PbSe and PbS are almost identical,[38] it is expected that the electron-phonon coupling is the dominating effect responsible for the reduction of dE_g/dT in alloyed CQDs. A minor contribution might be also assigned to a reduction of a core/shell interface strain by a better crystallographic match. In any event, the low value of *dE/dT* in the alloyed CQDs suggests a thermal stability of the band edge properties, with a significant importance in various applications and in particular in solar energy panels.

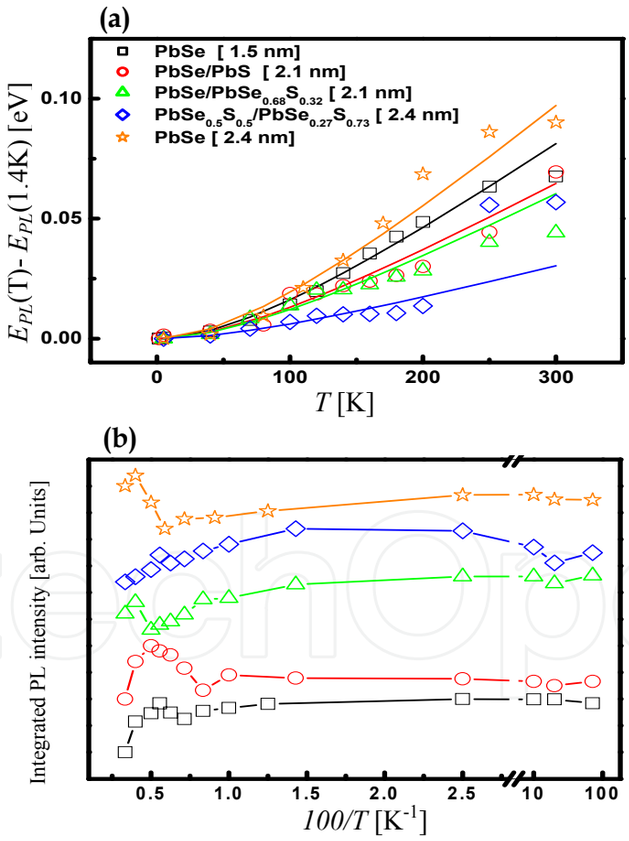

Fig. 7. Plot of the low cw-PL band emission peak energy relative to that at 1.4 K ($E_{PL}(T)$-$E_{PL}(1.4\ K)$) versus the temperature T of the samples mentioned in the legend (a). The symbols designate the experimental points, while the solid lines are the best fit curves; Plot of the integrated PL intensity versus *100/T* (b) of the samples presented in Panel (a). The solid lines here are drawn to guide the eye.

Figure 7 (b) demonstrates plots of the PL integrated intensity of the low energy cw-PL band *versus 100/T*. The plots show a similar tendency, including a plateau at the temperature range > 10 K to ~ 150 K, followed by low quenching of the intensity by an exciton-phonon interaction at higher temperatures, a typical behavior of a direct band gap semiconductor.[39] However, the trend is interrupted in two distinct points: (i) occurrence of unusual climax in the intensity profile at a temperature between 150 K to 250 K, appearing at higher temperature in c/sh and c/a-sh, compared with that of the primary cores, but with a very small effect in a-c/a-sh CQDs. This abnormal climax was previously explained[21] as a thermal activation between dark and bright states, with activation energy (ΔE_a) close to the LO phonon energy ($LO_{(PbSe)}$ = 16.8 meV, $LO_{(PbS)}$ = 26 meV). The values of ΔE_a of the investigated samples are listed in Table 3, spanning a range that is in close agreement to the suggested theoretical values of the dark-bright splitting in pure PbSe cores;[27] (ii) unexplained a minor decrease of the intensity <10 K with an activation energy ~ 0.4 meV, way below the acoustic phonon energy (LA, TA ~ 4-6 meV).[40] Worth to note, that the best fit shown in Panel (a) also show some deviation from perfection > 150 K, in correlation with the abrupt climax shown in Panel (b), due to a change in the emission mechanism from a dark to a bright state emission.

Molecular formula of CQDs	R_s [nm]	dE/dT [meV/K]	ΔE_a [meV]
PbSe	1.5	0.32	15.51
PbSe/PbS	2.1	0.17	17.23
$PbSe/PbSe_{0.68}S_{0.32}$	2.1	0.15	15.51
$PbSe_{0.5}S_{0.5}$/ $PbSe_{0.27}S_{0.73}$	2.4	0.06	-
PbSe	2.4	0.48	21.54
Bulk material	dE_g/dT [meV/K]		
PbSe	0.51		
PbS	0.52		

Table 3. An energy band-gap temperature coefficient dE/dT and thermal activation energy ΔE_a of PbSe core, PbSe/PbS c/sh, $PbSe/PbSe_xS_{1-x}$ c/a-sh and $PbSe_yS_{1-y}/PbSe_xS_{1-x}$ a-c/a-sh CQDs.

3. Thermally activated photoluminescence processes in PbS CQDs

For deeper understanding of the thermally activated emission processes in $PbSe_yS_{y-1}/PbSe_xS_{1-x}$ hetero-structures we also examined pure PbS CQDs with equevalent sizes. In the recent years a progress towards achieving a detailed understanding of emission in PbS has been made.[41-46] However, important challenges still remain, thus providing a strong motivation to study the fundamental physics of fluorescence in this semiconductor. The investigated PbS CQDs were prepared by colloidal chemistry, according to the procedures given in Ref. [43] and will be described in Section 5.2. The room temperature absorption and cw -PL spectra of PbS CQDs, with diameters between 2.2 and 3.5 nm (all dispersed in GS), are shown in Figure 8, while a representative HR-TEM image of a single CQD is shown in

the Inset. The crystallinity and composition of the materials were investigated by recording their HR-TEM images, revealing the formation of spherical CQDs with a high quality rock salt structure. The absorption spectra are comprised of the $1S_e$-$1S_h$ exciton transitions varying between 1.55 to 1.2 eV, corresponding to CQDs with a diameter between 2.2 to 3.5 nm and blue-shifted upon the decrease of diameter. Also, the $1S_e$-$1S_h$ exciton bands are blue-shifted with respect to that of the bulk exciton at 0.32 eV. The excitonic emission bands have a full width at half-maximum (FWHM) of about 200 meV, with E_s of 250 meV for the 2.2 nm CQDs, which reduces gradually with the increase of the CQDs size. For 3.5 nm CQDs E_s is 50 meV.

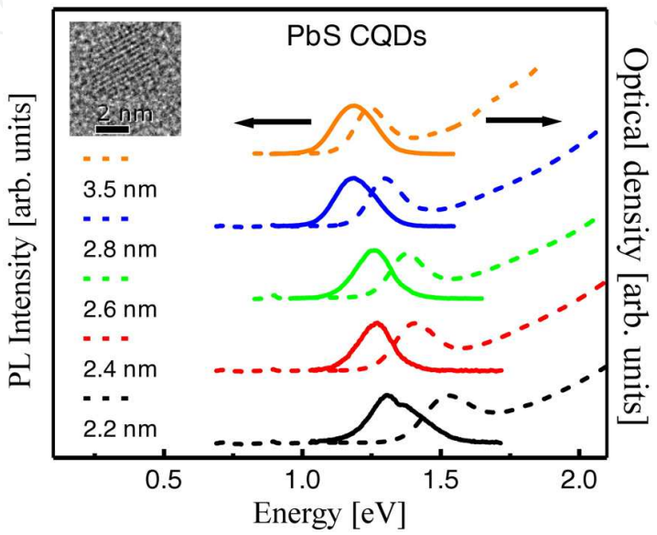

Fig. 8. Room temperature absorption (dash lines) and cw-PL spectra (solid lines) of PbS CQDs with an average diameter as indicated in the legend; Inset: HR-TEM image of a single PbS CQD; scale bar 2 nm.

This shift is the result of a split of the exciton manifold by the L-valley mixing and by the electron-hole exchange interaction, which further splits into dark and bright states. Figure 9(a) and 9(b) illustrate the cw-PL spectra of 2.6 and 3.5 nm PbS CQDs, respectively, dispersed in GS and recorded at various temperatures ranging from 4 K to 300 K.

At all temperatures the ground states exciton PL spectra of 2.6 nm CQDs are nealy symmetric, while PL spectra of 3.5 nm PbS CQDs have an asymmetric shape (like those of the equivalent size PbSe and $PbSe_yS_{1-y}/PbSe_xS_{1-x}$ a-c/a-sh hetrostructures), showing variations with the change in the temperature of the emission peak energy, FWHM and in integrated PL intensity.

The evolution of the PL peak energy with the increase in temperature of 2.6 and 3.5 nm PbS CQDs are shown in Figure 10(a) by the symbols (see legend in the figure) and the solid lines which are best fitted curves using Varshni relation.[36] The plots reveal a blue shift of the exciton emission energy with the increase in the temperature and can mainly attribute to the increase in the band gap energy with temperature, typical to the small band-gap IV-VI semiconductors. A tangent line to the fitted curve evaluates the slope, revealing the temperature coefficient, $\alpha = dE/dT$. The best fit α parameter for the PbS CQDs vary between - 0.17 meV/K (for the 2.6 nm) to 0.22 meV/K (for the 3.5 nm) and are smaller to similar sizes PbSe CQDs.[21]

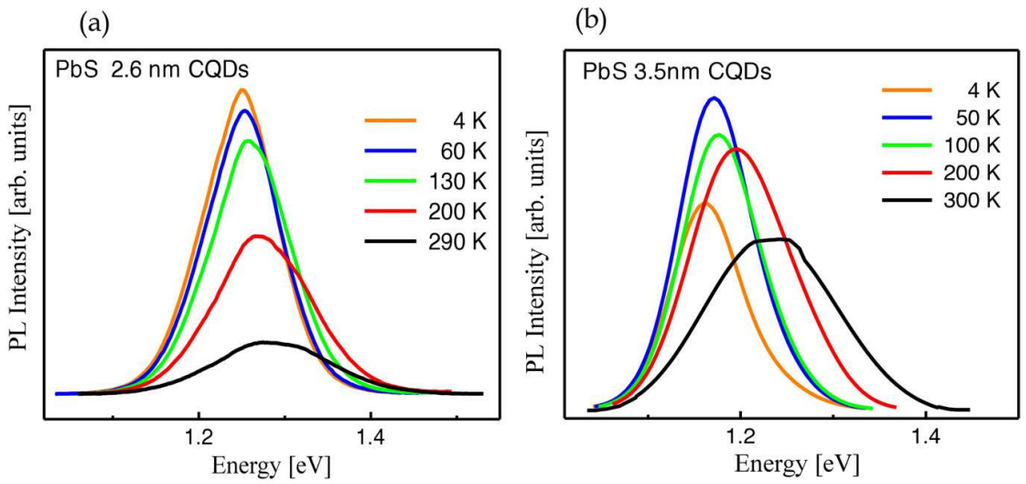

Fig. 9. Representative cw-PL spectra of PbS CQDs with diameter of 2.6 nm (a), and 3.5 nm (b) dispersed in GS and measured at various temperatures as indicated in the legend.

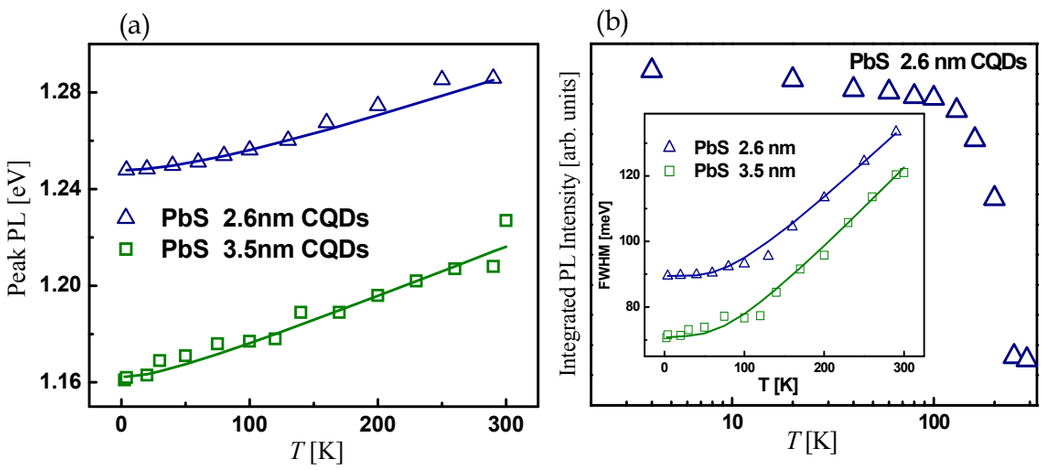

Fig. 10. Plots of the PL peak energy versus the temperature of PbS CQDs with dimensions as indicated in the legend (a); The solid lines represent a fit to a Varshni function[36] ;Integrated PL intensity of 2.6 nm PbS CQDs versus the temperature (b); inset: PL band's FWHM of PbS CQDs shown in Figure 9 versus the temperature. The solid lines represent a fit to the modified Bose–Einstein relation.[47]

Plot of the integrated PL intensity versus the temperature of 2.6 nm PbS CQDs is presented in Figure 10(b) and shows Arrhenius behavior. The activation energy extracted from the Arrhenius plot is 14 meV, and is smaller than the thermal activation energy ΔE_a obtained for PbSe CQDs'and $PbSe_yS_{1-y}/PbSe_xS_{1-x}$ a-c/a-sh CQDs heterostructures that are listed in Table 3.

The inset of Figure 10(b) represents a plot of the FWHM of PL spectra of the samples shown in Figure 10(a) as a function of temperature. The FWHM decreased with decreasing temperature and was best fitted to a modified Bose–Einstein relation given in Ref. [47]. The

experimental data reveal a reduction of the ground-state exciton broadening in the 2.6 nm CQDs in comparison with that in 3.5 nm PbS CQDs. The best fit curves are shown by the solid line in the figure. The values that were obtained by the best fit parameters are: inhomogeneous broadening parameter Γ_{inh} (taken as $\Gamma_o(T)$ at 0 K) varies between 70-90 meV depending on the CQDs' size, acoustic phonon coupling σ=0.016 meV/K , optical phonon coupling Γ_{LO}=56 meV. The LO-phonon energy E_{LO} was extracted from Raman measurements (not shown here) and is about 23 meV. The values obtained from Bose-Einstein relation are with accordance to those presented in the literature.[41]

Representative transient PL curves of 3.5 nm PbS CQDs in GS, recorded at various temperatures, are shown in Figure 11(a). These curves were fitted to a single exponent decay curve, $I_{(t)}$= A exp(–t/ τ_0), showing an obvious change with variation of T.

The best-fit lifetime's τ_0 of 2.6 and 3.5 nm PbS CQDs versus T are plotted in Figure 11(b), revealing a moderate decrease of the lifetime from 5.2 to 4.0 μs for 2.6 nm and from 6.5 to 5 μs for 3.5 nm PbS CQDs when T increases from 2.4 to 100 K. A steeper decrease of the lifetime is observed when T increases from 120 to 290 K. At all temperature the τ_0 are longer than those of 2.6 nm PbS QDs.[44]

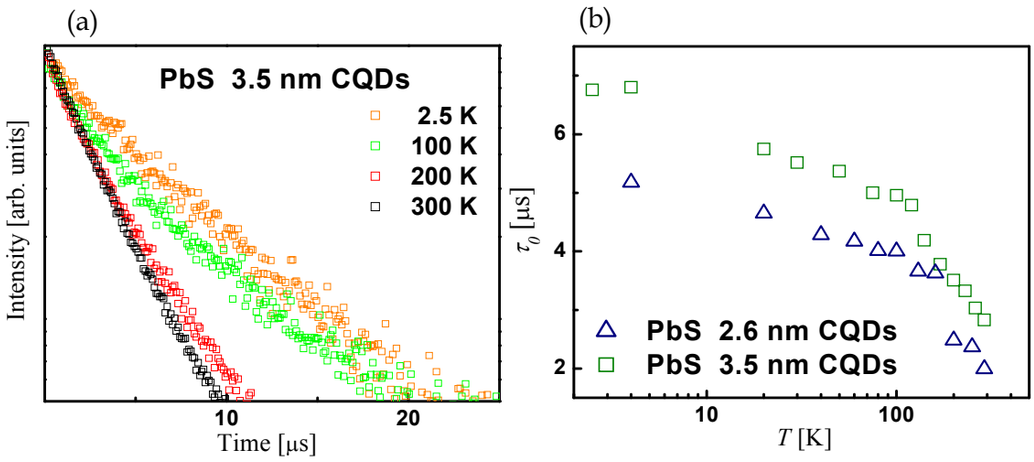

Fig. 11. Transient PL curves of 3.5 nm PbS CQDs dispersed in GS and recorded at various temperatures, as indicated in the legend (a); Plots of the lifetime, τ_0, versus T of PbS CQDs shown in Figure 9.

Spectrally resolved transient PL of 2.6 and 3.5 nm PbS CQDs measured at three different points of the PL band at various temperatures are shown in Figure 12(a) and 12(b). The arrows pointing to three different points of PL energy: red arrow- energy of the PL peak; black arrow – energy at the half PL intensity from the blue side of the PL, while the blue arrow is the energy at the half PL intensity from the red side of the PL. The obtained results reveal two emission bands with different τ_0 temperature dependent behaviour: the higher energy band τ_0 increase moderate with decrease of T from 290 to 4 K, while the low energy band show steeper τ_0 increase with decrease of T. This behavior suggests that the two band composed PL could correspond to bright and dark states induced by exchange interaction or to the two lowest valley-valley manifold exitonic states.

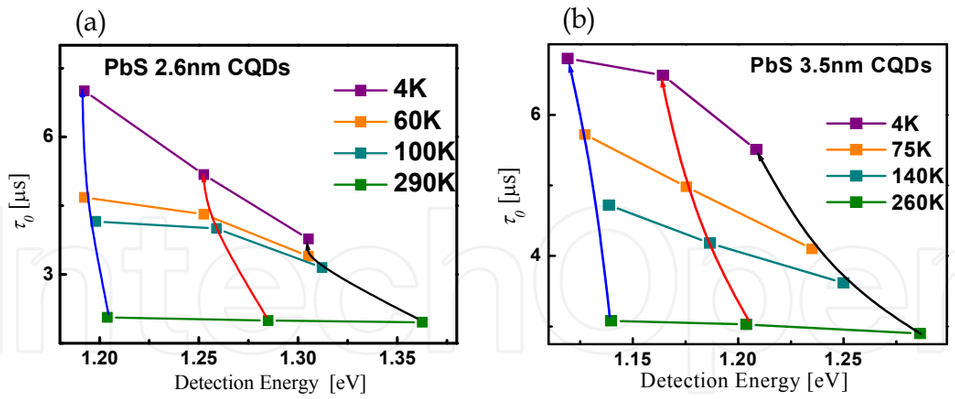

Fig. 12. Plots of the measured τ_0 versus the detection energy across the PL spectrum, of 2.6 (a) and 3.5 nm (b) PbS CQDs, measured at various temperatures (4-290 K) as indicated in the legends. The arrows pointing to three different points of PL energy: red arrow- energy of the PL peak; black arrow – energy at the half PL intensity from the blue side of the PL, while the blue arrow is the energy at the half PL intensity from the red side of the PL.

4. Theoretical prediction of the electronic properties of heterostructed QDs

The electronic band structure of the heterostructures (with/without alloy composition) quantum dots (QDs) was evaluated, using a k*p model, considering specific features, related to the discontinuity of the effective mass, crystal potential and dielectic constant at the core/shell, as well as at the shell/surrounding interface. The evaluation also considered anisotropy of effective masses, particularly in the IV-VI semiconductors. The evaluations explored interesting properties, associated with charge distribution between the core and the shell, effective electron-hole spatial separation, probability of transitions, coulomb interactions and tunability of band-edge and remote states' energy.[23, 48] Pre-engineering of the electronic band structure is done by theoretical consideration (of spherical particles alone for the moment), covering all cases, when, either the core or shell or both has alloy composition (see scheme in Figure 13). A few special points should be considered: anisotropy in effective mass (typical for IV-VI semiconductors), as well as the fact that each physical parameter dependents on its position (r) across the dot, and also may vary smoothly at the core/shell and the shell/surrounding interfaces, with a smoothing factor γ. The Hamiltonian was adjusted to the discontinuity at the PbSe/PbS interface by the appropriate choice of the kinetic energy term, ensuring probability current conservation and continuity of the envelope functions. In addition, the Hamiltonian potential energy term, included the heterostructure band offset, abrupt for the c/sh structure, but considered as a smooth function for the c/a-sh QDs.[49] Presumably, the smooth potential profile reflects the nature of the interface region in alloyed materials with gradient composition, being an extension of the standard treatment for semiconductor heterostructures. The overall band offset was chosen as that of the corresponding bulk PbSe and PbS materials (where the valence band maximum of bulk PbS lies 0.025 eV above that of PbSe, while the conduction band minimum lies 0.155 eV above that of PbSe). Diagonalization of the envelope function Hamiltonian yielded the electron and hole wavefunctions, as well as a good approximation of the energy values of the conduction and valence-band's states. The heterostructures

investigated are ternary core or c/sh QDs, having a general formula $PbSe_xS_{1-x}/PbSe_yS_{1-y}$, covering the following cases: (a) x = y = 1 or x = y = 0 refers to a simple core PbSe or PbS, respectively; (b) 0 < x = y < 1 is a homogenous alloy core; (c) x = 1 and y = 0 is a simple PbSe/PbS c/sh; (d) x = 1 (y = 1) and y ≠ 0 (x ≠ 0) is a complex c/sh QD, when either the core or the shell has a homogenous alloyed composition. A schematic drawing of a ternary QD is shown in Figure 13. R_c and R_s designate the radius of a core and a c/sh QD, respectively.

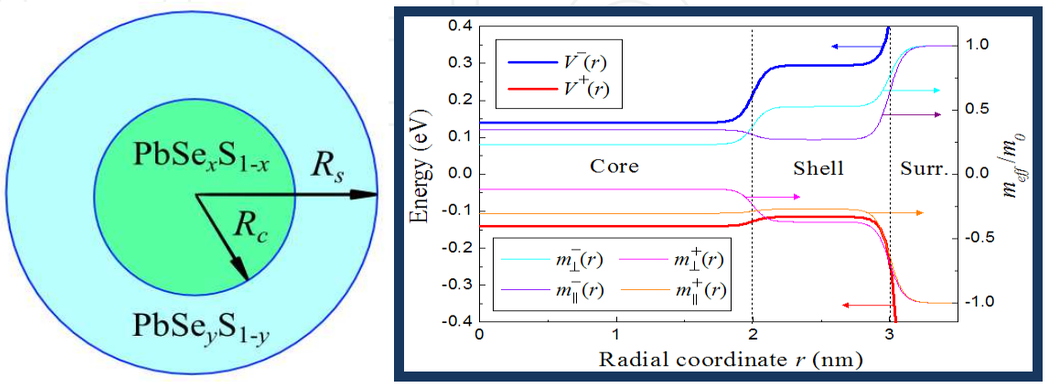

Fig. 13. Schematic drawing of a spherical c/sh $PbSe_xS_{1-x}/PbSe_yS_{1-y}$ QD. R_c and R_s are the core and the total radii, respectively. Radial variation of the bulk material parameters in spherical PbSe/PbS QD (R_c=2 nm, R_s=3 nm).

Three-dimensional plots of the electron and hole distribution functions on (111) cut-plane for a pure core (Panel (a)), c/sh QDs (Panels (b) and (c)) and c/a-sh (Panels (d) and (e)) of equivalent R_s, are shown in Figure 14. Panels (f) and (g) show the electron and the hole distribution for a c/a-sh with R_c=3 nm and R_s=5 nm. In the case of a pure core structure, the distribution of electron and hole is virtually identical, thus Panel (a) describes either one of the carriers. The choice of the (111) plane is made for the calculation convenience only, and is equivalent to choosing any other crystallographic plane for the distribution representation, since the ground state wavefunctions are spherically symmetric. These plots reveal a distinct trend, in which the lowest energy hole state, $|1/2,1\rangle$ (1/2 denotes the total angular momentum j of the state, and ±1 corresponds to the parity π), is more delocalized with respect to its counter partner, the lowest energy electron state $|1/2,-1\rangle$, in c/sh and c/a-sh QDs, characteristic of *quasi*-type II configuration at the band edge. This electronic distribution explains the experimental observations shown in Figure 2 of the gradual red-shift of the absorption spectra with the increase of the shell width . The electron and hole spatial distribution functions in c/sh CQDs shown in Figure 14(b) and 14(c) suggest that the distribution of both carriers is similar to that of a c/a-sh structure (Figure 14(d) and 14(e)); however, the distribution differs from the case of a simple core QD of comparable total size (Figure 14(a)). The calculations show that for heterostructured particles with R_c< 3 nm the energies of the lowest lying electron levels exceed the potential barrier height (either abrupt or gradual), located at the interface between the core and the shell, thus significantly reducing the effect of quantum confinement induced by the shell layer. On the other hand, in the case of larger c/sh or c/a-sh particles the electron energy is lower than the barrier height, thus enforcing the confinement (and subsequently the localization) of the electron in

the core region (*cf.* Figure 14(b) and 14(f)). However, the energy difference between the valence band edges of PbSe and PbS is almost an order of magnitude smaller than that between the conduction band edges, hence the hole distribution is influenced by the shell to a much lesser extent (*cf.* Figure 14(c) and 14(g)).

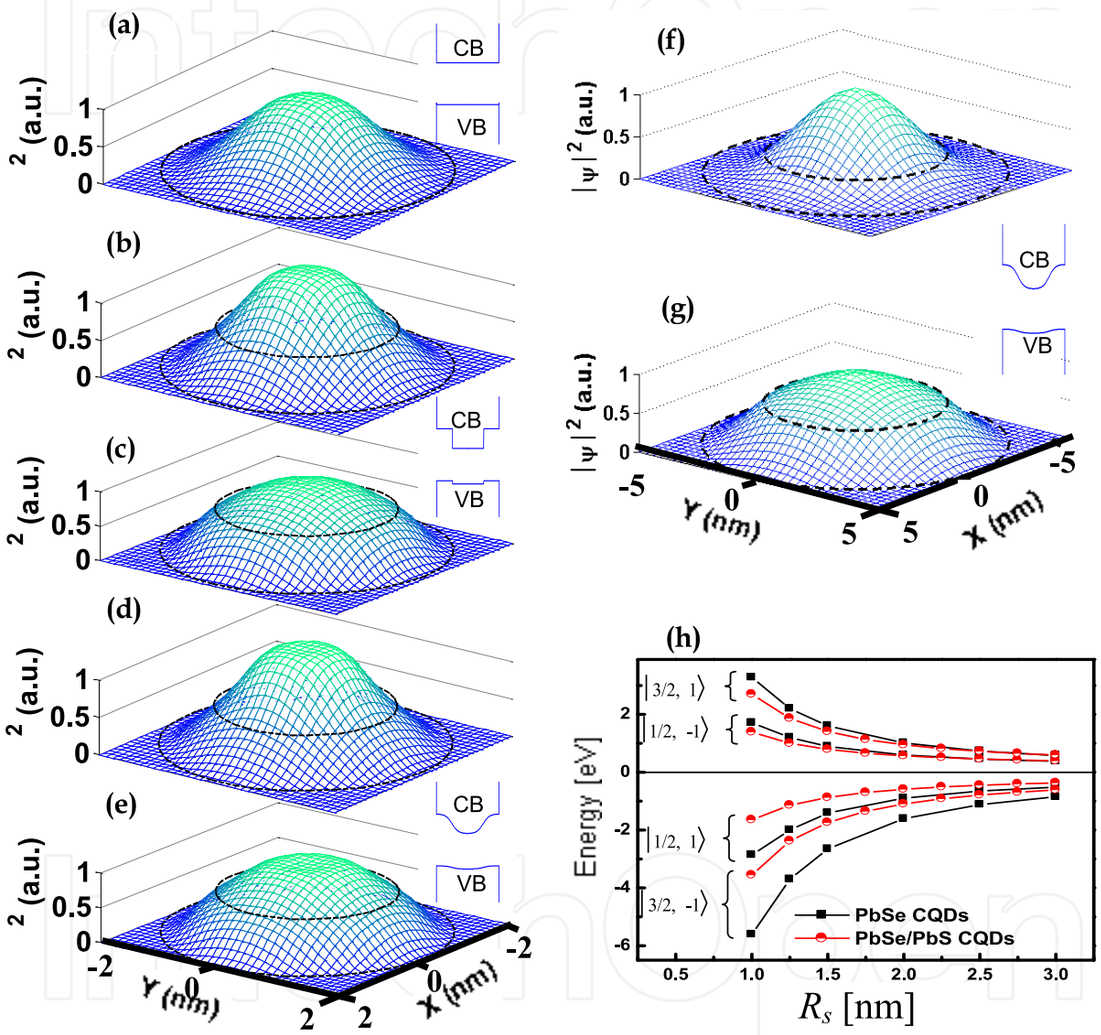

Fig. 14. Probability density on the (111) cut-plane for electron and hole in (a) PbSe QDs, R_s=2.4 nm. (b) Electron and (c) hole in PbSe/PbS CQDs, R_c=1.5 nm, R_s=2.4 nm. (d) Electron and (e) hole in c/a-sh QDs, R_c =1.6 nm, R_s =2.4 nm. (f) Electron and (g) hole in c/a-sh QDs, R_c =3 nm, R_s =5 nm (Both dashed circles, outer and inner, represent the external particle boundary and the core/shell interface location, respectively). The insets marked VB (valence band) and CB (conduction band) schematically represent the radial potential energy profile used in the calculation in each case. (h) Energy as a function of R_s of two lowest states of electron and hole in PbSe core and PbSe/PbS c/sh QDs with R_s / R_c =3/2.

Figure 14(h) displays the calculated energy of two lowest energy states versus the R_s of core and c/sh QDs with R_s / R_c =3/2. This Figure reveals a pronounced influence of the shell on the energy levels of the carriers.

In the case of a c/sh structure, both the electron and hole levels are lowered in energy relative to a core structure of the same size, with a larger influence on the hole levels. In the framework of this model the energy levels of c/a-sh structures are almost identical to those of c/sh, hence are not shown here. This finding is consistent with the experimental observation of the red-shift in the emission energy of the c/sh and c/a-sh heterostructures, relative to the cores of corresponding size. The theoretical $|1/2,1\rangle \rightarrow |1/2,-1\rangle$ transition energies (which is the first excitonic transition) are listed in Table 1 and are compared with the experimental absorption band edge energies, with a close agreement for QDs with R_s> 1.5 nm (Apparently, the accuracy of the model is not satisfactory for very small sizes due to the breakdown of the major assumption that the envelope function is slowly varying on the scale of the unit cell). The model reproduced the band edge energies of the QDs with relatively close agreement with the experiment, as well as predicted varying delocalization extent of the electrons in the lowest conduction band. The explanation of the reported variation of various physical properties of c/sh and c/a-sh heterostructures would demand further theoretical considerations (e.g., mass anisotropy, exchange interactions), which are beyond the scope of the discussed model, however, will be done in the future.

Evolution of the ten lowest conduction and valence band levels as a function of structure and composition of QD with R_s are shown in Figure 15.

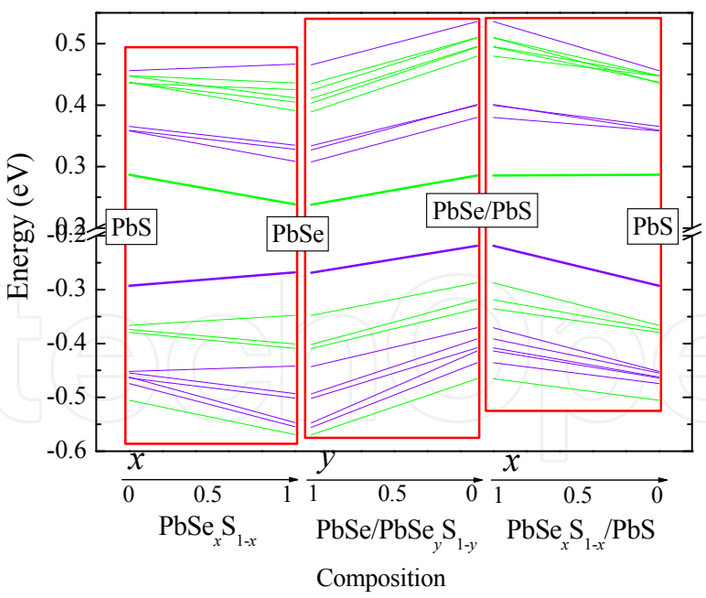

Fig. 15. Evolution of the energy of the conduction and valence band energy levels through a series of composition and structural changes, while maintaining a constant QD radius of 2.5 nm.

First, the QD structure evolves from PbS core to PbSe core via the intermediate alloyed $PbSe_xS_{1-x}$ structures (Left Panel). Next, the QD is divided into a 3 nm PbSe core and a 2 nm

thick $PbSe_ySe_{1-y}$ shell (*i.e.*, R_c=3 nm, R_s=5 nm). The shell composition then varies from y=1 to y=0, corresponding to a transition from pure PbSe to PbSe/PbS c/sh via intermediate $PbSe/PbSe_ySe_{1-y}$ c/sh structures (middle panel). Finally, the composition of the core constituent evolves from x=1 to x=0, corresponding to a transition from PbSe/PbS c/sh to a pure PbS core, which completes the cycle (Right Panel). States of even (+) and odd (-) parity are marked by purple and green lines, respectively. CB and VB correspond to the conduction and valence bands, respectively.

Figure 16 shows the energy levels (blue) and density of states (DOS) (green) of PbS (left panel), $PbSe_{0.5}S_{0.5}$ (middle panel) and PbSe (right panel) having R_s=2.5 nm. The density of states calculated by broadening each energy level by 25 meV Gaussian. The composition is found to have a significant impact on the energy spectrum of spherical QDs (apart from the band gap energy). For instance, when looking at the all three cases of $PbSe_xS_{1-x}$ core structures of the same size, in $PbSe_{0.5}S_{0.5}$ the levels are arranged into more dense discrete groups, while in PbS and PbSe QDs they are more evenly distributed, as can be seen in Figure 16.

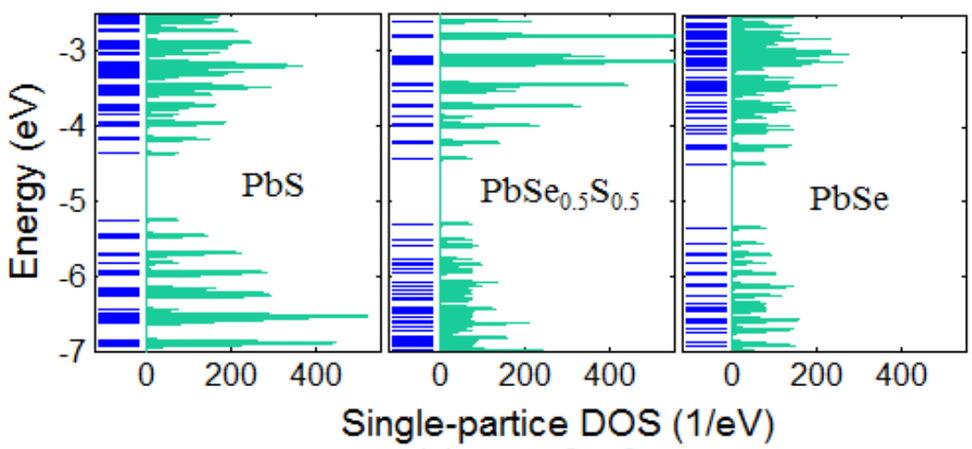

Fig. 16. Single-particle energy levels (blue) and density of states (green) of PbS (left panel), $PbSe_{0.5}S_{0.5}$ (middle panel) and PbSe (right panel) QDs having R_s=2.5 nm. The density of states calculated by broadening each energy level by 25 meV Gaussian.

It is intuitively clear that the origin of this composition-dependent variance of the DOS (that even reaches degeneracy in some cases) should be linked to some symmetry property of the system. In our case this property is the shape of the energy isosurface (EI) of $PbSe_xS_{1-x}$ bulk materials in the reciprocal space. As mentioned above, in the case of lead chalcogenides the general shape of the EI resembles a spheroid, having its principle axis in the L-direction, and it varies as a function of energy $E(\mathbf{k})$.

Calculated values of the fundamental gap energies E_g evaluated for various core and c/sh QDs, compared with experimental data are presented in Figure 17 and shows a qualitativly agreement between the theoretical and experimental results.

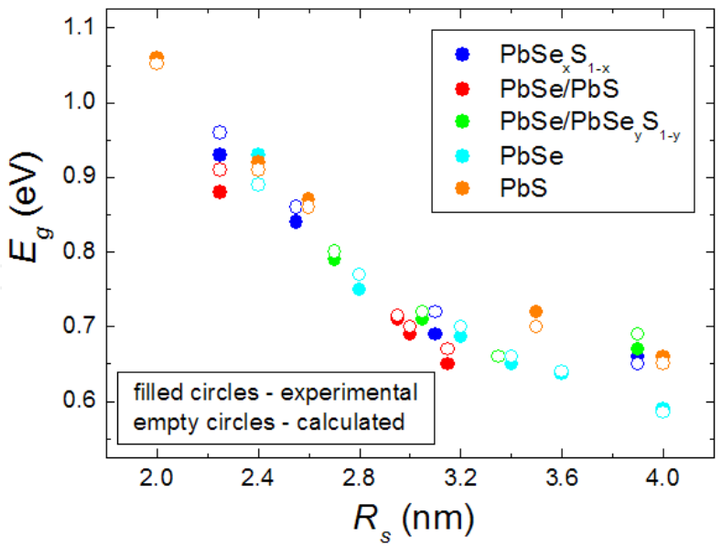

Fig. 17. Calculated (empty circles) and the corresponding experimental (filled circles) values of the band gap energies evaluated for several core and c/sh QDs.

5. Synthesis procedures and experimental techniques used for core/shell heterostructures with alloy components

5.1 Synthesis of PbSe, PbSe/PbS c/sh, PbSe/ $PbSe_xS_{1-x}$ c/a-sh and $PbSe_yS_{1-y}/PbSe_xS_{1-x}$ a-c/a-sh CQDs

The synthesis of core PbSe CQDs followed a modified procedure to that given by Murray et al.[50] , following the procedure given in[19] and including the preceding stages: (1) 0.71 gr of lead(II) acetate trihydrate [Pb-ac] ($Pb[CH_3COO]_2 \cdot 3H_2O$, GR, Merck) were dissolved in a solution composed of 2 mL diphenyl ether [PhEt] ($C_6H_5OC_6H_5$, 99%, Aldrich), 1.5 mL oleic acid (OA) ($CH_3(CH_2)_7$ $CHCH(CH_2)_7COOH$, 99.8%, Aldrich) and 8 mL TOP ($(C_8H_{17})_3P$, Tech, Aldrich), under standard inert conditions in the glove box, and were inserted into a three-neck flask (flask I); (2) 10 mL of PhEt were inserted into a three-neck flask (flask II) under the inert conditions of a glove box; (3) both flasks were taken out of the glove box, placed on a Schlenk line and heated under a vacuum to 100 - 120°C for an hour; (4) flask I was cooled to 45°C, while flask II was heated to 180 -210°C, both under a fledging of an argon gas; (5) 0.155 gr of selenium powder (Se, 99.995%, Aldrich) was dissolved in 2.0 mL TOP, forming a TOP:Se solution, under standard inert conditions of a glove box. Then, 1.7 mL of this solution was injected into flask I on the Schlenk line; (6) the content of flask I, containing the reaction precursors, was injected rapidly into the PhEt solution in flask II, reducing its temperature to 100 - 130°C, leading to the formation of PbSe CQDs within the first 15 min of the reaction. The described procedure produced nearly mono-dispersed CQDs with < 8% size distribution, with average size between 3 and 9 nm, controlled by the temperature and by the time duration of the reaction.

The preparation of PbSe/PbS c/sh CQDs by a two-injection process[19] begins with formation of core PbSe CQDs and their isolation from the initial reaction solution, according to the procedure described previolsy. Those core CQDs were re-dissolved in chloroform solution, forming a solution of 50 mg/mL weight concentration. The quality of 1.4 mL of TOP was

then added to the CQDs solution, while the chloroform molecules were removed by distillation under vacuum and heating at 60°C. In parallel, 0.2 gr of a Pb precursor, Pb-ac, was dissolved in a mixture of 2 mL PhEt, 1.5 mL of OA, and 8 mL of TOP, heated to 120°C for an hour, and then cooled to 45°C. Also, 0.03–0.10 gr of sulphur (S, 99.99 + %, Aldrich) was dissolved in 0.3 mL of TOP and was premixed with a PbSe core CQDs in a TOP solution. This mixture was injected into the Pb-ac solution. All reagents were then injected into a PhEt mother solution and kept on a Schlenk line at 180°C, causing a reduction in temperature of the mother solution to 120°C. The indicated chemical portions caused the precipitation of 1–3 monolayers of PbS shell over the PbSe core surface within the first 15 min of the reaction.

The preparation of PbSe/$PbSe_xS_{1-x}$ c/a–sh and $PbSe_xS_{1-x}$/$PbSe_yS_{1-y}$ a-c/a-sh structures[19] is nearly identical to that of the core PbSe CQDs, described previosly using a single injection of the precursors into a single round flask. However, step (5) was altered by the use of an alternative chalcogen precursor stock solution. A stock solution of Se and S was prepared by mixing 0.15 gr Se dissolved in 1.4 mL TOP, with 0.03–0.10 gr S dissolved in 0.3 mL TOP. The amount of S in the new stock solution corresponded to a stoichiometric amount of 1–2 ML of the PbS compound. Thus, the mole ratio of the precursors Pb:Se:S ranged from 1:1:0.5 to 1:1:1.3. Aliquots were drawn periodically from the mother solutions while quenching process to RT terminated the CQDs' growth. They were isolated from the aliquots solution by the addition of methanol, and by centrifugation. The isolated CQDs were further purified by dissolving them in chloroform, followed by filtering several times through a 0.02 micron membrane. A preliminary injection of Pb/Se/S ions ratio of 1/1/0.5 led to the nucleation of a pure PbSe core, due to the faster reactivity of the Se precursors at the nucleation stage. However, the increase of the S/Se ratio (S/Se> 1.5/1) enabled an immediate integration of both elements with the nuclei (monitored already in the first aliquot). Further aliquots revealed a gradient increase of the S/Se ratio when moving from the interface toward the exterior surface. For simplicity, the samples were labeled as $PbSe_yS_{1-y}$/$PbSe_xS_{1-x}$.

5.2 Synthesis of PbS CQDs

PbS CQDs were prepared according to literature procedure.[43] The lead oleate precursor was prepared by heating 0.09 g PbO in 4 ml OA under N_2 at 120^0C for 1h. A solution of 42 µl bis(trimethylsilyl)sulfide (TMS) in 2 ml octadecene (ODE) was injected into the vigorously stirring lead oleate solution. The final particle size was controlled by injection temperature (120-150 ^{0}C), where lower temperature leads to smaller sizes, and by varying the Pb:OA molar ratios (2:32 to 2:4, where the total volume of lead oleate solution was kept at 4 ml by dilution with ODE). The reaction was quenched by cooling it to RT and the CQDs were precipitated with acetone, then subsequently redispersed in chloroform and precipitated again.

5.3 Experimenthal methods

The morphology and crystallography of the colloidal CQDs were examined by X-ray diffraction, TEM, HR-TEM and SAED. The TEM specimens were prepared by injecting small liquid droplets of the solution on a copper grid (300 mesh) coated with amorphous carbon film and then dried at room temperature. The elemental analysis were examined by EDAX, and inductively coupled plasma atomic emission spectroscopy (ICP-AES).

The absorption spectra of the samples were recorded on a JASCO V-570 UV-VIS-NIR spectrometer. The cw-PL spectra were obtained by exciting the samples with a tunable Ti:Sapphire laser, (E_{exc} = 1.48-1.80 eV). The PL spectra of the materials studied were recorded at a temperature range of 1.4 K to 300 K, while immersing the samples in a variable temperature Janis cryostat, and detecting the emission with an Acton Spectrapro 2300i monochromator, which was equipped with a cooled InGaAs CCD or cooled Ge photo detector. The transient PL curves were recorded by exciting the samples with a Nd:YAG laser, (E_{exc} = 1.17 eV). The measurements utilized a laser flux <0.1 mJ/cm^2, corresponding to a photon fluence of j_p~10^{11} photons/cm^2 per pulse. Considering the absorption cross-section of σ_0~10^{-15} cm^2, measured in reference,[14] the number of photo-generated excitons is given by $<N_0>= j_p \cdot \sigma_0$, and estimated to be $10^{-4}<<1$, ensuring the generation of single excitons. The transient-PL curves were monitored by a photon multiplier tube, Hamamatsu NIR-PMT H10330-75. The measurements were carried out at temperature range from 1.4 K to 300 K. The PL quantum yield was measured utilizing integrating sphere technique described by Friend.[51] A solution of CQDs was placed inside an integrating sphere and excited by a monochromatic light. Luminescence spectra were detected by a fiber-coupled spectrometer equipped with a liquid nitrogen-cooled Ge photo detector. The entire system response was normalized against a calibrated detector, and care was taken to ensure that the sample absorption was more than 20%.

5.4 Storage conditions

The $PbSe_yS_{1-y}/PbSe_xS_{1-x}$ a-c/a-sh ($0<x<1;0<y<1$) CQDs were stored either in a various solutions (chloroform, hexane) or were embedded in a polymer film or dissolved in a GS (2,2,4,4,6,8,8,-heptamethyl-nonane) for the optical measurements. The polymer-CQDs solution was prepared by mixing PbSe CQDs in chloroform solution with poly-methyl-methacrylate (PMMA) ($[–CH_2C(CH_3)(CO_2CH_3)–]_n$, analytical grade, Aldrich) polymer solution. The resultant mixture was spread on a quartz substrate and dried over 24 h to a uniform film. The stability of these CQDs was examined over a period of time by recording the absorption spectra and following the consistency of the low exciton energy. Plots of this exciton energy versus time suggest that the exciton energy in the core samples is blue-shifted by ~ 400 meV over a period of days for the CQDs kept in a chloroform solution. Such a blue-shift, however, occurs over months for the samples kept as dry powders. On the other hand, the energy shift is smaller for the PbSe/PbS c/sh samples, and even nearly disappeared for the CQDs coated with three PbS shell monolayers. It is presumed that the exciton energy blue-shift is due to oxidation of the surface, and a decrease of the effective size of the core. Obviously, the penetration of oxygen through the PbS shell is reduced with the growth of the shell width. Furthermore, storage of the CQDs in a nitrogen environment nearly eliminates any spectral drift over a period of months, even extending to two or three years. It should be noted that most of the optical measurements were carried out at cryogenic temperatures, inducing a He gas environment around the samples. But unpublished results determined degradation of the samples when exposed to intense pulsed UV radiation, which is avoided completely in the current study.

6. Conclusion and future directions

Unique alloyed c/sh heterostructures, such as $PbSe_yS_{1-y}$ /$PbSe_xS_{1-x}$, ($0<x\leq1$; $0<y\leq1$) were developed, offering good crystallographic and dielectric match at the c/sh interface,

regulating carriers' delocalization and/or charge separation by tunability of the band off-set, showing an exceptionally high emission quantum yield, chemical stability, and an option to stabilize the emission intensity (blinking free behavior), as well as sustain the biexciton lifetime over a nanosecond. The last can be of a valuable benefit in the use of CQDs in gain devices and photovoltaic cells.

A smooth potential at the c/sh interface was applied here for the determination of the electronic structure of IV-VI CQDs, using a $\mathbf{k}\cdot\mathbf{p}$ model, covered a wide physical aspects, including an effective mass anisotropy, dielectric variation between the constituents, showing a ground for tailoring heterostructures with the desired composition and optical properties.

A thorough investigation of the optical properties was performed by following variable temperature cw- and transient spectrally resolved PL spectra, exploring energy shift, band edge temperature coefficient, alleviation of a dark-bright splitting (or exchange interaction), valley-valley interaction, emission quantum yield, and radiative lifetime of the $PbSe_yS_{1-y}$ /$PbSe_xS_{1-x}$ heterostructures, in comparison with the existing properties of the primary PbSe core CQDs. Temporally and spectrally resolved PL spectra provide more-systematic evidence of the two emissive centers nature. The results reflect the uniqueness of the electronic properties of the heterostructures, controlled by shell width and alloyed composition.

The discussed heterostructures could be of significant importance in applications where the CQDs' size is restricted, *e.g.*, biological markers or self-assembled CQDs in opto-electronic devices, while at the same time, there are stringent demands regarding the optical tunability. We showed that the restriction can be overcome by the discussed new strategies gaining property control using: (a) alloyed ternary or quaternary compounds, when all elements can be either distributed homogeneously or exhibit a graded composition along a selective direction; (b) c/sh heterostructures, comprised of a semiconductor core, covered by a shell, of another semiconductor, when the band-edge off-set at the core/shell interface, can be tuned from a type-I (when shell band-edge is rapping that of the core), through *quasi*-type-II, to a type-II (when, band-edge of the constituents are staggered) alignment. Moreover, one of the constituents (core or shell) may have alloyed composition.

7. Acknowledgment

The authors thank G. Kventsel for helpful discussions, providing many insightful comments, A. Bartnik and F. Wise for helpful discussions and guidance on the theoretical model, A. Efros for the useful scientific discussions, and O. Solomeshch for assistance in the quantum yield measurements. The authors acknowledge support from the Israel Science Foundation (Projects No. 1009/07 and No. 1425/04), the USA-Israel Binational Science Foundation (No. 2006-225), and the Ministry of Science (No. 3-896).

8. References

[1] Steigerwald, M. L.; Brus, L. E., Semiconductor crystallites: a class of large molecules. *Accounts of Chemical Research* 1990, *23* (6), 183-188.

[2] Peng, X.; Manna, L.; Yang, W.; Wickham, J.; Scher, E.; Kadavanich, A.; Alivisatos, A. P., Shape control of CdSe nanocrystals. *Nature* 2000, *404* (6773), 59-61.

[3] Akamatsu, K.; Tsuruoka, T.; Nawafune, H., Band Gap Engineering of CdTe Nanocrystals through Chemical Surface Modification. *Journal of the American Chemical Society* 2005, *127* (6), 1634-1635.

[4] Ma, W.; Luther, J. M.; Zheng, H.; Wu, Y.; Alivisatos, A. P., Photovoltaic Devices Employing Ternary PbS_xSe_{1-x} Nanocrystals. *Nano Letters* 2009, *9* (4), 1699-1703.

[5] Bailey, R. E.; Nie, S., Alloyed Semiconductor Quantum Dots: Tuning the Optical Properties without Changing the Particle Size. *Journal of the American Chemical Society* 2003, *125* (23), 7100-7106.

[6] Piven, N.; Susha, A. S.; Döblinger, M.; Rogach, A. L., Aqueous Synthesis of Alloyed CdSexTe1-x Nanocrystals. *The Journal of Physical Chemistry C* 2008, *112* (39), 15253-15259.

[7] Erwin, S. C.; Zu, L.; Haftel, M. I.; Efros, A. L.; Kennedy, T. A.; Norris, D. J., Doping semiconductor nanocrystals. *Nature* 2005, *436* (7047), 91-94.

[8] Danek, M.; Jensen, K. F.; Murray, C. B.; Bawendi, M. G., Synthesis of Luminescent Thin-Film CdSe/ZnSe Quantum Dot Composites Using CdSe Quantum Dots Passivated with an Overlayer of ZnSe. *Chemistry of Materials* 1996, *8* (1), 173-180.

[9] Ivanov, S. A.; Piryatinski, A.; Nanda, J.; Tretiak, S.; Zavadil, K. R.; Wallace, W. O.; Werder, D.; Klimov, V. I., Type-II Core/Shell CdS/ZnSe Nanocrystals: Synthesis, Electronic Structures, and Spectroscopic Properties. *Journal of the American Chemical Society* 2007, *129* (38), 11708-11719.

[10] Piryatinski, A.; Ivanov, S. A.; Tretiak, S.; Klimov, V. I., Effect of Quantum and Dielectric Confinement on the Exciton-Exciton Interaction Energy in Type II Core/Shell Semiconductor Nanocrystals. *Nano Letters* 2006, *7* (1), 108-115.

[11] Oron, D.; Kazes, M.; Banin, U., Multiexcitons in type-II colloidal semiconductor quantum dots. *Physical Review B* 2007, *75* (3), 035330.

[12] Mamutin, V. V.; et al., Molecular beam epitaxy growth methods of wavelength control for InAs/(In)GaAsN/GaAs heterostructures. *Nanotechnology* 2008, *19* (44), 445715.

[13] Lauhon, L. J.; Gudiksen, M. S.; Wang, D.; Lieber, C. M., Epitaxial core-shell and core-multishell nanowire heterostructures. *Nature* 2002, *420* (6911), 57-61.

[14] Dorfs, D.; Franzl, T.; Osovsky, R.; Brumer, M.; Lifshitz, E.; Klar, T. A.; Eychmuller, A., Type-I and Type-II Nanoscale Heterostructures Based on CdTe Nanocrystals: A Comparative Study. *Small* 2008, *4* (8), 1148-1152.

[15] Nonoguchi, Y.; Nakashima, T.; Kawai, T., Tuning Band Offsets of Core/Shell CdS/CdTe Nanocrystals. *Small* 2009, *5* (21), 2403-2406.

[16] Sashchiuk, A.; Langof, L.; Chaim, R.; Lifshitz, E., Synthesis and characterization of PbSe and PbSe/PbS core-shell colloidal nanocrystals. *Journal of Crystal Growth* 2002, *240* (3-4), 431-438.

[17] Stouwdam, J. W.; Shan, J.; van Veggel, F. C. J. M.; Pattantyus-Abraham, A. G.; Young, J. F.; Raudsepp, M., Photostability of Colloidal PbSe and PbSe/PbS Core/Shell Nanocrystals in Solution and in the Solid State. *The Journal of Physical Chemistry C* 2006, *111* (3), 1086-1092.

[18] Xu, J.; Cui, D.; Zhu, T.; Paradee, G.; Liang, Z.; Wang, Q.; Xu, S.; Wang, A. Y., Synthesis and surface modification of PbSe/PbS core–shell nanocrystals for potential device applications. *Nanotechnology* 2006, *17* (5428).

[19] Brumer, M.; Kigel, A.; Amirav, L.; Sashchiuk, A.; Solomesch, O.; Tessler, N.; Lifshitz, E., PbSe/PbS and PbSe/PbSe$_x$S$_{1-x}$ Core/Shell Nanocrystals. *Advanced Functional Materials* 2005, *15* (7), 1111-1116.

[20] Lifshitz, E.; Brumer, M.; Kigel, A.; Sashchiuk, A.; Bashouti, M.; Sirota, M.; Galun, E.; Burshtein, Z.; Le Quang, A. Q.; Ledoux-Rak, I.; Zyss, J., Air-Stable PbSe/PbS and PbSe/PbSe$_x$S$_{1-x}$ Core/Shell Nanocrystal Quantum Dots and Their Applications. *The Journal of Physical Chemistry B* 2006, *110* (50), 25356-25365.

[21] Kigel, A.; Brumer, M.; Maikov, G. I.; Sashchiuk, A.; Lifshitz, E., Thermally Activated Photoluminescence in Lead Selenide Colloidal Quantum Dots. *Small* 2009, *5* (14), 1675-1681.

[22] Bartnik, A. C.; Wise, F. W.; Kigel, A.; Lifshitz, E., Electronic structure of PbSe/PbS core-shell quantum dots. *Physical Review B* 2007, *75* (24), 245424.

[23] Maikov, G. I.; Vaxenburg, R.; Sashchiuk, A.; Lifshitz, E., Composition-Tunable Optical Properties of Colloidal IV−VI Quantum Dots, Composed of Core/Shell Heterostructures with Alloy Components. *ACS Nano* 2010, *4* (11), 6547-6556.

[24] Moreels, I.; Lambert, K.; Smeets, D.; De Muynck, D.; Nollet, T.; Martins, J. C.; Vanhaecke, F.; Vantomme, A.; Delerue, C.; Allan, G.; Hens, Z., Size-Dependent Optical Properties of Colloidal PbS Quantum Dots. *ACS Nano* 2009, *3* (10), 3023-3030.

[25] Garrett, M. D.; Dukes Iii, A. D.; McBride, J. R.; Smith, N. J.; Pennycook, S. J.; Rosenthal, S. J., Band Edge Recombination in CdSe, CdS and CdSxSe1−x Alloy Nanocrystals Observed by Ultrafast Fluorescence Upconversion: The Effect of Surface Trap States. *The Journal of Physical Chemistry C* 2008, *112* (33), 12736-12746.

[26] Huang, Y. H.; Cheng, C. L.; Chen, T. T.; Chen, Y. F.; Tsen, K. T., Studies of Stokes shift in InxGa1?xN alloys. *Journal of Applied Physics* 2007, *101*.

[27] An, J. M.; Franceschetti, A.; Zunger, A., The Excitonic Exchange Splitting and Radiative Lifetime in PbSe Quantum Dots. *Nano Letters* 2007, *7* (7), 2129-2135.

[28] Allan, G.; Delerue, C., Confinement effects in PbSe quantum wells and nanocrystals. *Physical Review B* 2004, *70* (24), 245321.

[29] Harbold, J. M.; Wise, F. W., Photoluminescence spectroscopy of PbSe nanocrystals. *Physical Review B* 2007, *76* (12), 125304.

[30] Tischler, J. G.; Kennedy, T. A.; Glaser, E. R.; Efros, A. L.; Foos, E. E.; Boercker, J. E.; Zega, T. J.; Stroud, R. M.; Erwin, S. C., Band-edge excitons in PbSe nanocrystals and nanorods. *Physical Review B* 2010, *82* (24), 245303.

[31] Schaller, R. D.; Crooker, S. A.; Bussian, D. A.; Pietryga, J. M.; Joo, J.; Klimov, V. I., Revealing the Exciton Fine Structure of PbSe Nanocrystal Quantum Dots Using Optical Spectroscopy in High Magnetic Fields. *Physical Review Letters* 2010, *105* (6), 067403.

[32] Chappell, H. E.; Hughes, B. K.; Beard, M. C.; Nozik, A. J.; Johnson, J. C., Emission Quenching in PbSe Quantum Dot Arrays by Short-Term Air Exposure. *The Journal of Physical Chemistry Letters* 2011, *2* (8), 889-893.

[33] Abel, K. A.; Qiao, H.; Young, J. F.; van Veggel, F. C. J. M., Four-Fold Enhancement of the Activation Energy for Nonradiative Decay of Excitons in PbSe/CdSe Core/Shell versus PbSe Colloidal Quantum Dots. *The Journal of Physical Chemistry Letters* 2010, *1* (15), 2334-2338.

[34] Liu, H.; Guyot-Sionnest, P., Photoluminescence Lifetime of Lead Selenide Colloidal Quantum Dots. *The Journal of Physical Chemistry C* 2010, *114* (35), 14860-14863.
[35] van Driel, A. F.; Allan, G.; Delerue, C.; Lodahl, P.; Vos, W. L.; Vanmaekelbergh, D., Frequency-Dependent Spontaneous Emission Rate from CdSe and CdTe Nanocrystals: Influence of Dark States. *Physical Review Letters* 2005, *95* (23), 236804.
[36] Varshni, Y. P., Temperature dependence of the energy gap in semiconductors. *Physica* 1967, *34* (1), 149-154.
[37] Olkhovets, A.; Hsu, R. C.; Lipovskii, A.; Wise, F. W., Size-Dependent Temperature Variation of the Energy Gap in Lead-Salt Quantum Dots. *Physical Review Letters* 1998, *81* (16), 3539.
[38] Madelung, O., *Semiconductors: Data Handbook*. 3rd ed.; Springer: 2004.
[39] Morello, G.; De Giorgi, M.; Kudera, S.; Manna, L.; Cingolani, R.; Anni, M., Temperature and Size Dependence of Nonradiative Relaxation and Exciton−Phonon Coupling in Colloidal CdTe Quantum Dots. *The Journal of Physical Chemistry C* 2007, *111* (16), 5846-5849.
[40] Upadhyaya, K. S.; Yadav, M.; Upadhyaya, G. K., Lattice Dynamics of IV–VI Ionic Semiconductors: An Application to Lead Chalcogenides. *physica status solidi (b)* 2002, *229* (3), 1129-1138.
[41] Turyanska, L.; Patane, A.; Henini, M.; Hennequin, B.; Thomas, N. R., Temperature dependence of the photoluminescence emission from thiol-capped PbS quantum dots. *Applied Physics Letters* 2007, *90* (10), 101913-3.
[42] Sargent, E. H., Infrared photovoltaics made by solution processing. *Nat Photon* 2009, *3* (6), 325-331.
[43] Hines, M. A.; Scholes, G. D., Colloidal PbS nanocrystals with size-tunable near-infrared emission: Observation of post-synthesis self-narrowing of the particle size distribution. *Advanced Materials* 2003, *15* (21), 1844-1849.
[44] Moreels, I.; Justo, Y.; De Geyter, B.; Haustraete, K.; Martins, J. C.; Hens, Z., Size-Tunable, Bright, and Stable PbS Quantum Dots: A Surface Chemistry Study. *Acs Nano* 2011, *5* (3), 2004-2012.
[45] Fernée, M. J.; Jensen, P.; Rubinsztein-Dunlop, H., Bistable Switching between Low and High Absorbance States in Oleate-Capped PbS Quantum Dots. *ACS Nano* 2009, *3* (9), 2731-2739.
[46] Fernée, M. J.; Jensen, P.; Rubinsztein-Dunlop, H., Origin of the Large Homogeneous Line Widths Obtained from Strongly Quantum Confined PbS Nanocrystals at Room Temperature. *The Journal of Physical Chemistry C* 2007, *111* (13), 4984-4989.
[47] O'Donnell, K., Temperature dependence of semiconductor band gaps. *Appl. Phys. Lett.* 1991, *58* (25), 2924.
[48] Trinh, M. T.; Polak, L.; Schins, J. M.; Houtepen, A. J.; Vaxenburg, R.; Maikov, G. I.; Grinbom, G.; Midgett, A. G.; Luther, J. M.; Beard, M. C.; Nozik, A. J.; Bonn, M.; Lifshitz, E.; Siebbeles, L. D. A., Anomalous Independence of Multiple Exciton Generation on Different Group IV−VI Quantum Dot Architectures. *Nano Letters* 2011, *11* (4), 1623-1629.
[49] Cragg, G. E.; Efros, A. L., Suppression of Auger Processes in Confined Structures. *Nano Letters* 2009, *10* (1), 313-317.

[50] Murray, C. B.; Shouheng, S.; Gaschler, W.; Doyle, H.; Betley, T. A.; Kagan, C. R., Colloidal synthesis of nanocrystals and nanocrystal superlattices. *IBM J. Res. & Dev.* 2001, *45*, 47.

[51] de Mello, J. C.; Wittmann, H. F.; Friend, R. H., An improved experimental determination of external photoluminescence quantum efficiency. *Advanced Materials* 1997, *9* (3), 230-232.

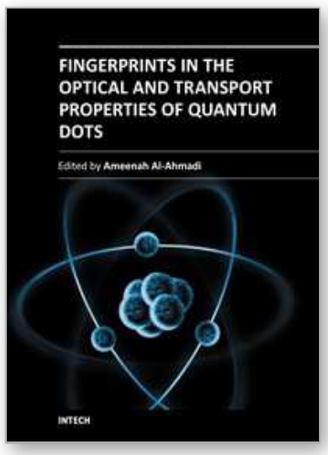

Fingerprints in the Optical and Transport Properties of Quantum Dots

Edited by Dr. Ameenah Al-Ahmadi

ISBN 978-953-51-0648-7
Hard cover, 468 pages
Publisher InTech
Published online 13, June, 2012
Published in print edition June, 2012

The book "Fingerprints in the optical and transport properties of quantum dots" provides novel and efficient methods for the calculation and investigating of the optical and transport properties of quantum dot systems. This book is divided into two sections. In section 1 includes ten chapters where novel optical properties are discussed. In section 2 involve eight chapters that investigate and model the most important effects of transport and electronics properties of quantum dot systems This is a collaborative book sharing and providing fundamental research such as the one conducted in Physics, Chemistry, Material Science, with a base text that could serve as a reference in research by presenting up-to-date research work on the field of quantum dot systems.

How to reference

In order to correctly reference this scholarly work, feel free to copy and paste the following:

Efrat Lifshitz, Georgy I. Maikov, Roman Vaxenburg, Diana Yanover, Anna Brusilovski, Jenya Tilchin and Aldona Sashchiuk (2012). Temperature-Dependent Optical Properties of Colloidal IV-VI Quantum Dots, Composed of Core/Shell Heterostructures with Alloy Components, Fingerprints in the Optical and Transport Properties of Quantum Dots, Dr. Ameenah Al-Ahmadi (Ed.), ISBN: 978-953-51-0648-7, InTech, Available from: http://www.intechopen.com/books/fingerprints-in-the-optical-and-transport-properties-of-quantum-dots/temperature-dependent-optical-properties-of-colloidal-iv-vi-quantum-dots-composed-of-core-shell-

INTECH
open science | open minds

InTech Europe
University Campus STeP Ri
Slavka Krautzeka 83/A
51000 Rijeka, Croatia
Phone: +385 (51) 770 447
Fax: +385 (51) 686 166
www.intechopen.com

InTech China
Unit 405, Office Block, Hotel Equatorial Shanghai
No.65, Yan An Road (West), Shanghai, 200040, China
中国上海市延安西路65号上海国际贵都大饭店办公楼405单元
Phone: +86-21-62489820
Fax: +86-21-62489821

IntechOpen